Biomimetic amniotic/silicone-based bilayer membrane for corneal tissue engineering

Esmaeili, Zahra; Nokhbedehghan, Zeinab; Alizadeh, Sanaz; majidi, Jila; Chahsetareh, Hadi; Daryabari, Seyed Hashem; Nazm-Bojnourdi, Maryam; Kadkhodaie, Majid; Ghaffari, Maryam; Hashemi, Ali

Total number of authors:
15

Published in:
Materials and Design

Link to article, DOI:
10.1016/j.matdes.2023.112614

Publication date:
2024

Document Version
Publisher's PDF, also known as Version of record

Materials & Design 237 (2024) 112614

Contents lists available at ScienceDirect

Materials & Design

journal homepage: www.elsevier.com/locate/matdes

Biomimetic amniotic/silicone-based bilayer membrane for corneal tissue engineering

Zahra Esmaeili [a,b,1], Zeinab Nokhbedehghan [a,b,1], Sanaz Alizadeh [b,c], Jila majidi [b,c], Hadi Chahsetareh [d], Seyed-Hashem Daryabari [e], Maryam Nazm-Bojnourdi [f], Majid Kadkhodaie [g], Maryam Ghaffari [h], Ali Hashemi [i], Hatef Ghasemi Hamidabadi [j,k,*], Ahmad Ahmadzadeh Amiri [l], Hajar Nasiri [b,c], Alireza Dolatshahi-Pirouz [m], Mazaher Gholipourmalekabadi [a,b,n,*]

[a] Department of Medical Biotechnology, Faculty of Allied Medicine, Iran University of Medical Sciences, Tehran, Iran
[b] Cellular and Molecular Research Center, Iran University of Medical Sciences, Tehran, Iran
[c] Department of Tissue Engineering & Regenerative Medicine, Faculty of Advanced Technologies in Medicine, Iran University of Medical Sciences, Tehran, Iran
[d] Department of Life Science Engineering, Faculty of New Science and Technologies, University of Tehran, Iran
[e] Vision Health Research Center, Semnan University of Medical Sciences, Semnan, Iran
[f] Mazandaran University of Medical Sciences, Department of Anatomical Science, Mazandaran, Sari, Iran
[g] Department of Genetics, Faculty of Advanced Science and Technology, Tehran Medical Sciences, Islamic Azad University, Tehran, Iran
[h] Biomaterials Group, Faculty of Biomedical Engineering (Centre of Excellence), Amirkabir University of Technology, Tehran, Iran
[i] Department of Microbiology, School of Medicine, Shahid Beheshti University of Medical Sciences, Tehran, Iran
[j] Department of Anatomy & Cell Biology, Faculty of Medicine, Mazandaran University of Medical Sciences, Sari, Iran
[k] Immunogenetic Research Center, Department of Anatomy & Cell Biology, Faculty of Medicine, Mazandaran University of Medical Sciences, Sari, Iran
[l] Department of Ophthalmology, Clinical Research Development Unit of Bu-Ali Sina Hospital, Faculty of Medicine, Mazandaran University of Medical Sciences, Iran
[m] Department of Health Technology, Technical University of Denmark, 2800 Kgs. Lyngby, Denmark
[n] NanoBiotechnology & Regenerative Medicine Innovation Group, Noavarn Salamat ZHINO (PHC), Tehran, Iran

ARTICLE INFO

Keywords:
Polydimethylsiloxane (PDMS)
Corneal tissue engineering
Amniotic membrane
Silicone dressing
Bilayer

ABSTRACT

Amniotic membrane (AM) is an effective and widely used dressing in ocular injuries to reconstruct the cornea. Due to its low mechanical strength, high biodegradation rate, and difficult handling, its usage in medical interventions remains challenging. In this study, decellularized AM was covered with an ultrathin layer of Polydimethylsiloxane (PDMS) through a spinning method, which in turn resulted in an ultrathin (less than 80 μm in thickness) bilayer corneal wound dressing membrane with improved mechanical behavior and transparency. The biomechanical, biological, and antibacterial properties of the bilayer membranes were measured both *in vitro* and *in vivo*. The optimized microsized membrane was applied on a corneal defect wound created in a rabbit model to evaluate the corneal healing. The results demonstrated a significant decrease in degradation rate, improved mechanical properties, and AM/PDMS transparency compared with AM. The corneal transparency improved until 21 days post-surgery in AM/PDMS group. Histological evaluations revealed that AM/PDMS had better epithelial delaminated cell morphology. The results of the RT-PCR showed a significant increase in MMP9, a significant decrease in Col1A1, TGF-β1, TNF-α and IL-6 in both AM and AM/PDMS compared with control wounds. This study suggessts AM/PDMS membrane as an excellent corneal wound dressing.

1. Introduction

The cornea is a frontal and layered part of the eye which is transparent and essential for eyesight. The thickness of the human cornea varies from person to person; however, the average has been reported to be about 0.5 mm [1,2]. Specifically, it is composed of five different layers; Epithelium, Bowman's layer, Stroma, Descemet's membrane, and Endothelium, respectively [3]. Different types of injuries may disrupt normal vision in different parts of the cornea [4]. Burns, and foreign bodies, lacerations and perforations, are the most common

* Corresponding authors.
E-mail addresses: h.ghasemi@mazums.ac.ir (H. Ghasemi Hamidabadi), mazaher.gholipour@iums.ac.ir (M. Gholipourmalekabadi).
[1] Equally contributed to this study.

https://doi.org/10.1016/j.matdes.2023.112614
Received 17 August 2023; Received in revised form 18 December 2023; Accepted 26 December 2023
Available online 30 December 2023

trauma which could destroy epithelium to endothelium layers of the cornea [5]. Depending on the depth of damage, healing processes could be completed rapidly or more challenging [1]. Generally speaking, after corneal damage, under normal conditions, the epithelial layer initiates self-repair through complicated cellular and molecular processes [6]. However, therapeutic interventions should help accelerate the healing process of corneal injuries to full regeneration and less damage to vision [7–9]. Currently, there are some standard and new interventions like lubricants, contact lenses, patching, dressings, autologous serum, amniotic membrane grafts, and in some cases, corneal transplants which can improve the regeneration and healing process [7,10,11]. Recently, tissue engineering has opened a new window to ameliorating tissue damage, especially in the case of pre-corneal defects. A wide range of natural and synthetic biomaterials have been developed as scaffolds for tissue repair, including collagen, silk, Polycaprolactone (PCL), Polycarbonate urethane (PCU), and amniotic membrane (AM) [2,12]. The AM is the placenta's innermost membrane, and consists of epithelium, protein, and extracellular matrix (ECM) structures [13]. AM has been used widely in corneal tissue regeneration due to its anti-inflammatory and re-epithelialization properties since the 1990 s [14–16]. Besides its merits in the field, it is still challenging to use because of its high biodegradation rate and low mechanical strength, which makes folding easily in the wet state and difficult to handle [13,17–19]. Polydimethylsiloxane, known as PDMS, belongs to the silicone elastomer group [20,21]. It is a transparent, gas permeable, cost-effective, cytobiocompatible, and hydrophobic polymer with high mechanical strength, thermal and chemical stability [22–24]. These properties have made it widely used in the biomedical industry [25] in applications including microfluidic instruments [26,27], contact lenses [28,29], and patterning [30,31]. These extraordinary properties also make it amenable as a composite biomaterial and scaffold for tissue engineering applications. In this study, we developed an ultrathin bilayer membrane based on AM and PDMS using a centrifugal force with improved biomechanical properties and corneal wound healing potential *in vitro* and *in vivo*.

2. Materials and methods

Ethical approval

The ethical committee approved this study at the Mazandaran University of Medical Sciences (MAZUMS ethical code: IR.MAZUMS.4.REC.1402.17206) to use human amniotic membrane and animal investigations based on the national guidelines and the World Medical Association Declaration of Helsinki.

2.2. Study design

The design of this study is illustrated in Fig. 1. *In vitro* investigations included bilayer membrane fabrication, biomaterial, and cellular characterization. Human amniotic membrane (AM) was decellularized, characterized by histological observation, and fixed on the glass slide. In the next step, PDMS was blended with a curing agent and poured on the AM in different volumes and rotation speeds. The bilayer membrane were fully characterized *in vitro*. The optimized bilayer membrane was applied on a corneal defect model created in the rabbit model. After 21 days, the implanted cornea tissues were collected for histological and molecular investigations.

2.3. Preparation, decellularization and characterization of amniotic membrane

The human amniotic membrane (AM) was prepared, decellularized, and characterized by a protocol described in our previously published article [32]. AM was achieved through informed consent from the placenta of caesarian section mothers. The candidates were screened for

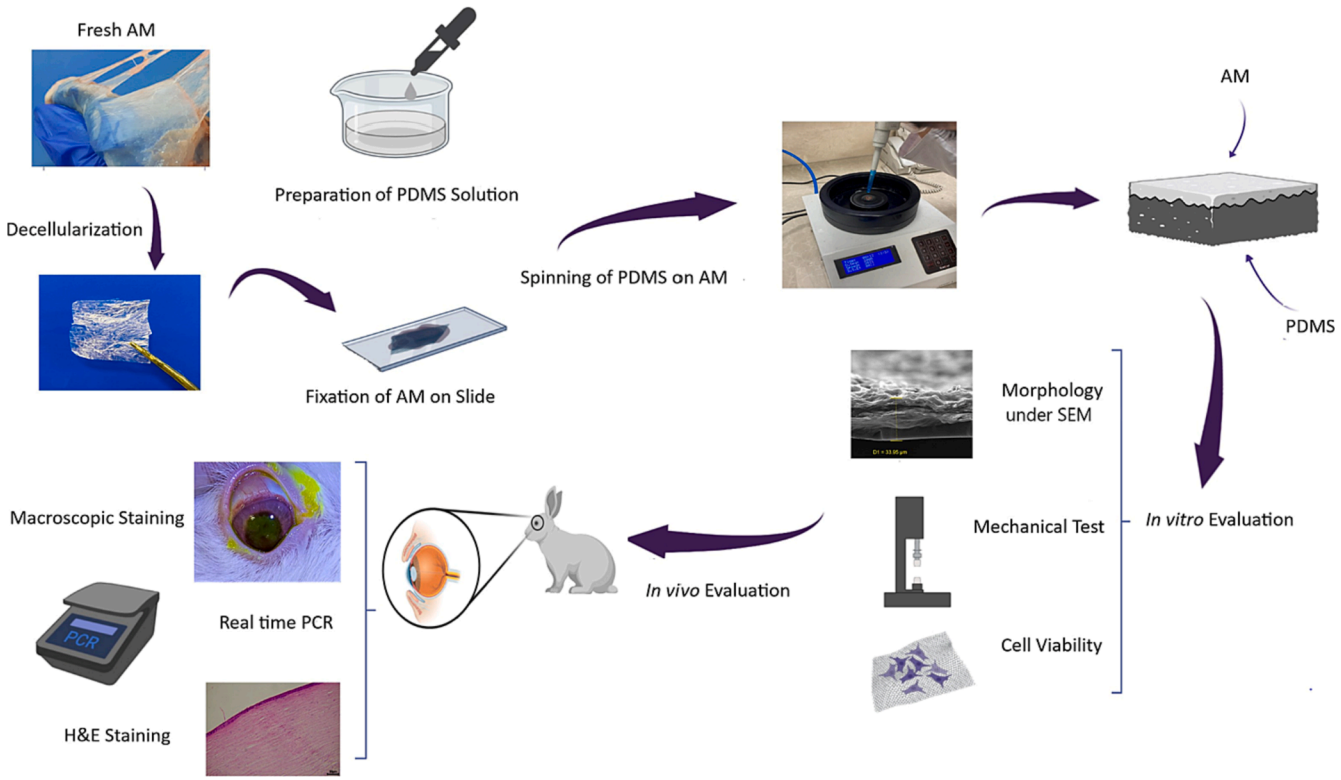

Fig. 1. Schematic preparation of amniotic membrane-silicone ultrathin bilayer membrane (AM/PDMS). Human amniotic membrane (AM) was decellularized, and fixed on the glass slide in wet form. Then, the decellularized AM was coated with different volumes of PDMS using different rotation speeds of the spinning apparatus. The bilayer membrane was deeply characterized *in vitro* and *in vivo* for treatment of corneal tissue defect in a rabbit model.

hepatitis virus type C and type B, human immunodeficiency virus type II, cytomegalovirus, toxoplasmosis, syphilis, and gonorrhea. AM and chorion layers were separated under sterile conditions. After that, the AM was decellularized with 0.2 % EDTA and 0.5 M NaOH using a protocol described in our previously published study. The decellularized AM was verified by DAPI and hematoxylin and eosin (H&E) staining [33].

2.4. Fabrication of amniotic membrane-silicone ultrathin bilayer membrane

Polydimethylsiloxane (PDMS, SYLGARD® 184, RTV, and Dow Corning, USA) was used to fabricate the amniotic membrane-silicone ultrathin bilayer membrane. Silicone resin and curing agent were mixed at a ratio of 10:1 and heated for 30–35 min at 45 °C. The wet AM was cut to 1.5 * 1.5 mm dimensions, fixed on the glass slide, and placed on a spinning apparatus (Backer, Laboratory Equipment, Iran). Different volumes of PDMS mixtures were directly poured on AM, and AM/silicone was spun at different rotation speeds to fabricate a bilayer membrane. In Table 1, the experimental group conditions for fabricating different AM/PDMS membranes are listed.

2.5. Characterization of the amniotic membrane-silicone ultrathin bilayer membrane

2.5.1. Morphology under SEM

A study of scaffold morphology was conducted under a scanning electron microscope (SEM, AIS2100; Seron Technology, Uiwang-si, Gyeonggi-do, South Korea) [34] at an acceleration voltage of 15 kV. All samples were coated with a layer of gold prior to scanning. A SEM software program was used to measure the membranes' cross-sectional thickness.

2.5.2. Mechanical properties

The mechanical characteristics of the scaffolds were tested by a mechanical tester (SANTAM; STM-20, Iran). A scaffold with rectangular shape (20 × 10 mm^2) was pulled in a gauge length of 25 mm at a crosshead speed of 10 mm/min until failure. The load cell was 60 N. Tensile strength, Young's modulus and elongation at break were determined [35]. Moreover, the suture retention strength of the scaffold was evaluated. The specimen was prepared in the same dimension and orientation (20 × 10 mm^2). A half-loop of suture material 3–0 was placed in a 2 mm away from the direction of pulling. The rate was 10 mm/min. The bilayer membrane with higher mechanical properties and thinner thickness was considered an optimized ultrathin bilayer membrane and subjected to further biomechanical, biological, and *in vivo* investigations.

2.5.3. Water contact angle (WCAs)

The optimized bilayer membrane hydrophilicity and hydrophobicity were determined using the contact angle goniometer (CA-500A, Sharif Solar, Iran). Briefly, a drop of deionized water was deposited on the surface of the scaffold, and the static contact angle was evaluated. The average of three repetitions served as the measurement for each sample.

Table 1
The PDMS volume and spinning rotation speed were used to prepare the bilayer membrane.

Sample	Speed rotation (rpm)	Volume (μl)
AM/PDMS 1500/100	1500	100
AM/PDMS 1500/150	1500	150
AM/PDMS 1500/200	1500	200
AM/PDMS 2000/100	2000	100
AM/PDMS 2000/150	2000	150
AM/PDMS 2000/200	2000	200
AM/PDMS 2500/100	2500	100
AM/PDMS 2500/150	2500	150
AM/PDMS 2500/200	2500	200

2.5.4. Transparency

The transparency of AM and AM/PDMS (optimized bilayer scaffold) in wet and dry forms was observed by placing them on glass surface-printed letters. The membranes were photographed using a camera Canon750D, and the letter resolution under the membrane was observed and compared between groups [36].

2.5.5. Degradation rate (weight loss%)

Biodegradation rate ***(weight loss%)*** was assessed by immersing the membranes in PBS (GIBCO) and monitoring the samples' weight loss. The scaffolds (AM, PDMS, and AM/PDMS) were carefully weighed (W_{init}) first, then immersed in a PBS solution at 37 ^{O}C and pH 7.4 for up to 25 days and used the same medium without refreshing. Three samples were taken at 5-day time intervals, washed several times with deionized water to remove water-soluble inorganic ions, and vacuum-dried for 24 h. Then, the weight of samples was measured again (W_{deg}), and the weight loss (W_{loss}) was deliberated according to the following formula [37] (Eq1). Furthermore, the samples were selected from each group on days 7 and 14 of incubation. Finally, SEM was used to inspect the surface and thickness of the samples for degradation.

$$W_{loss} = [(W_{init} - W_{deg})/W_{init}] \times 100\ \%\ (1)$$

2.5.6. Cell-membrane interaction behaviors

For the corneal epithelial cells adhesion assay, the corneal epithelial cells (5 × 10^4 cells/well) were seeded on each side of the bilayer membrane, and then incubated at 37℃. After 72 h, all the samples were prepared for observation under SEM using our previous published protocol [38]. The attachment and distribution of corneal epithelial cells grown on AM and bilayer membrane was studied by staining the cells' nuclei with 4', 6-diamidino-2-phenylindole (DAPI, Sigma-Aldrich). A fluorescence microscope (Olympus BX51, Tokyo, Japan) was used to visualize the DAPI-stained nuclei of the cells. The effect of bilayer membrane on the rabbit's primary corneal epithelial cells viability was determined by MTT assay. The cells were cultured on AM/PDMS, AM, PDMS and cell culture well (control, 100 % cell viability) for 3 and 7 days in a Dulbecco's Modified Eagle's Medium (DMEM) supplemented with 10 % fetal bovine serum (FBS), 1 % penicillin, and streptomycin (all from GIBCO, UK). At each time interval, the cells were treated with MTT solution (10 % solution in DMEM, Sigma-Aldrich, USA) for 2 h, and then treated with dimethyl sulfoxide (DMSO, Sigma-Aldrich, USA) in a dark chamber for 20 min. The optical density of MTT formazan purple crystals was recorded at 590 nm wavelength. The percentage of viable corneal epithelial cells was calculated using the following equation [39] (Eq2):

$$\text{Cell viability (\%)} = (\text{Absorbance in treated wells/absorbance in control wells}) \times 100\ (2)$$

2.5.7. Antibacterial behavior

2.5.7.1. Disc diffusion. The bactericide property of AM and AM/PDMS *Acinetobacter baumannii* ATCC 19606 was determined by disk diffusion assay. The scaffolds (1*1 disks) were sterilized by UV irradiation and placed in the center of muller Hilton agar cultured with 0.5 Mcfarland concentration of bacteria. After 24 h incubation at 37 ℃, the bacterial growth inhibition zone around the AM and AM/PDMS was observed and measured using a ruler [40].

2.5.7.2. SEM. The presence of bacteria cultured on AM and AM/PDMS was determined by observation under SEM. For this purpose, the AM and AM/PDMS bilayer scaffold (1.5 cm*1.5 cm) were immersed in 500

μl of 0.5 McFarland (1.5 × 10 8 CFU/ml) bacterial suspension of *A. baumanii* (ATCC 19606) at 37 °C for 18 h. After removing the scaffolds, they were gently cleaned with PBS. Afterward, 2.5 % glutaraldehyde was used to fix the bacteria/scaffold constructs for 2.5 h, and the constructs were then dehydrated by adding alcohol graded series (30, 50, 70, 90, 96, and 100) for 20 min. The samples were then scanned under SEM to observe the presence of bacteria attached to the scaffolds [41].

2.5.8. Subcutaneous biocompatibility assay

The scaffolds were subcutaneously implanted in a mouse animal model to assess their biocompatibility. In this way, three NMRI male mice (6–8 weeks, 30 g) were used for each experimental group. The animals were kept in separate cages and maintained at 25 °C in light–dark periods of 12 h; free access to drinking water and food. Ketamine hydrochloride (0.1 mg/kg) and xylazine (0.01 mg/kg) (both from Sigma, USA) were injected intra peritoneal to anesthetize the animals. The back hair of the mice was shaved and the scaffolds (5 × 5 mm) were implanted subcutaneously. The mice were sacrificed by CO_2 asphyxiation at days 7 (short-term) and 21 (long-term) post-surgery, and the tissue was harvested and processed for H&E staining. The stained samples were viewed under light microscopy (Olympus, Tokyo, Japan) [42].

2.6. In vivo corneal defect model in rabbit

Three New Zealand white rabbits, weighing 2.0—2.5 kg, were purchased from the Pasteur Institute of Iran. Animals were anesthetized systemically with xylazine (10 $mg.kg^{-1}$) and ketamine (100 $mg.kg^{-1}$) (both from Sigma, USA). Additionally, a local anesthetic was performed with tetracaine hydrochloride eye drops 1 %. Each animal's left eye was considered as control eye. After general anesthesia, 4 mm diameter disk of Whatman filter paper was soaked in 30 % ethanol and fixed in the center of the cornea in the right eye of each animal for 90 s to create a corneal defect wound model [43,44]. The filter paper was removed, and the cornea's surface was immediately washed with 10 ml of standard sterile saline solution. The surface of the corneal epithelium was then scratched, and the corneal injuries were stained with fluorescein sodium solution (0.1 %) to measure the corneal epithelium defect size. UV sterilized scaffolds (AM alone and AM/PDMS) were implanted on the defected surface with a 10.0 nylon suture. After surgery, betamethasone and clobiotic eye drops were applied daily (continuously for 3–5 days) to prevent postoperative eye infection in rabbits.

2.7. In vivo corneal wound healing evaluations

2.7.1. Macroscopic staining

A fluorescein stain was used to examine the regeneration of corneal epithelium in the transplanted area. Fluores® eye examination test paper (Showa Yakuhin Kako, Tokyo, Japan) carefully placed on the lid margin. Many natural blinks were allowed to the recipients. A biomicroscope was used to examine the ocular surface under blue light irradiation. Additionally, the corneal epithelium was visually examined for damage.

2.7.2. Histological observations

The animal of each experimental group was sacrificed at 21 days postoperative. The corneal tissues (control and implanted with AM and AM/PDMS) were collected for routine histological evaluations. In brief, the corneas were fixed with formaldehyde (4 %), embedded in paraffin, and sectioned at 4 μm thicknesses. After dehydration of the samples, the slides were stained with H&E [45] and Masson's trichrome and observed under light microscopy (Olympus, Tokyo, Japan) to assess wound healing and collagen synthesis.

2.7.3. Gene expression

About 50 mg of the corneal tissue was collected on day 21 post-implantation. Total RNA was isolated using a commercial kit (Qiagen), in accordance with the manufacturer's instructions. Briefly, the corneal tissues were treated with lysis buffer, then RNA was purified, and reverse transcription was applied using random hexamer primers and qPCRBIO cDNA synthesis kit (Biosystems Ltd., London, UK). Real-time PCR (SYBR® Premix Ex Taq TM II, TaKaRa) was used to determine the relative expression of the target genes [46]. The primers used in this study are listed in Table 2. Relative expression of target genes was calculated based on the $2^{-\Delta\Delta Ct}$ method.

GAPDH (Glyceraldehyde-3-phosphate dehydrogenase), IL-6 (Interleukin 6), TNF-α (tumor necrosis factor alpha), TGF-β1 (Transforming growth factor beta 1), VEGF-A (Vascular endothelial growth factor A), MMP-9 (Matrix metallopeptidase 9), COL1A1 (Collagen Type I Alpha 1 Chain).

2.8. Statistical analysis

The Statistical analysis was assessed by two-way ANOVA and Fisher's LSD (GraphPad Prism ver. 9.0). $P < 0.05$ was deliberated as the level of significance. The number of samples for each group was 3, and the data were defined as mean ± SD.

3. Results

3.1. Decellularized amniotic membrane investigation

The results obtained from H&E and DAPI staining of fresh and decellularized AM are illustrated in Fig. 2. Micrographs confirmed that the decellularization process of AM was successfully performed, and the cells were completely removed from the tissue; in contrast, the cells' nuclei were clearly visualized in fresh (cellular) AM.

3.2. Characterization of amniotic membrane-silicone ultrathin bilayer membrane scaffold

3.2.1. Amniotic membrane-silicone ultrathin bilayer membrane morphology characterization

Cross-sectional view of the AM/PDMS samples was observed by SEM (Fig. 3A). The PDMS was homogenously injected, and distributed on the AM in different volumes and rotation speeds. Two layers are connected without any gap space. The average thickness of bilayer scaffolds was around 57.04 μm. According to the data presented in Fig. 3(B), the bilayer membrane prepared by 150 μl PDMS and 2000 rpm rotation speed had the thinnest thickness among the experimental groups. As shown in Fig. 3(C), the AM and PDMS surfaces were uniform without damage.

3.2.2. Tensile testing

Results of young's modulus, tensile strength, and elongation at break

Table 2
Real-Time PCR primer sequences.

Animal	Gene name	Sequence	Tm (℃)
Rabbit	GAPDH	F: 5′-AGACACGATGGTGAAGGTCG-3′ R:5′-TGCCGTGGGTGGAATCATAC-3′	60
Rabbit	IL-6	F: 5′-GAACAGAAAGGAGGCACTGG-3′ R: 5′- CTCCTGAACTTGGCCTGAAG −3′	58
Rabbit	TNF-α	F: 5′-AGCCCACGTAGTAGCAAACC-3′ R: 5′-TGAGTGAGGAGCACGTAGGA-3′	60
Rabbit	TGF-β1	F: 5′-TGCTGCTGCCTCTGCTGT-3′ R: 5′-GGCCTGGATGTGCTGTTGTC-3′	61
Rabbit	VEGF-A	F: 5′-AGTTCGAGGAAAGGGCAAGG-3′ R: 5′-ACGCGAGTCTGTGTTTTTGC-3′	60
Rabbit	MMP-9	F: 5′- CGGAGACGGGTATCCTTTCG-3′ R: 5′- CGGCGTTTCCAAAGTACGTG-3′	60
Rabbit	COL1A1	F: 5′-CAGCGGCTCCCCATTTTCTA-3′ R:5′-ATCTCAGCTCGCATAGCACC-3′	60

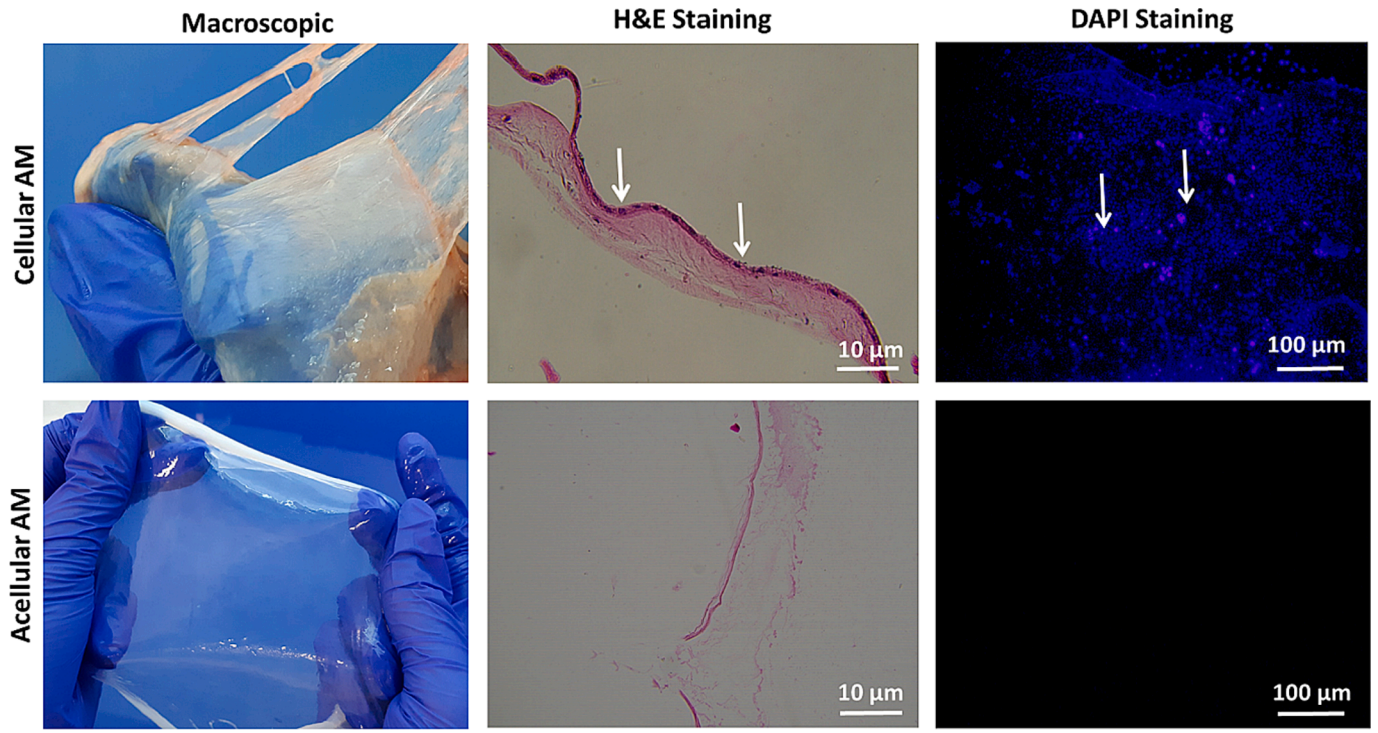

Fig. 2. Decellularization and characterization of AM. Staining fresh and decellularized AMs with H&E and DAPI confirmed the successful removal of the cells from tissues. Arrows indicate H&E- and DAPI-stained cells.

for all the fabricated bilayer scaffolds are shown in Fig. 4(A). The mechanical properties were reported based on the spin speed of 1500, 2000, and 2500 rpm and the PDMS volumes of 100, 150, and 200 µl, respectively. In this way, the elongation at break of samples with the spin speed of 1500 rpm was 20.1 %, 15.1 %, and 10.1 %, Young's modulus was 86.43 MPa, 62.56 MPa, and 55.07 MPa, and the tensile strength was 9.3 MPa, 8.7 MPa, and 7.3 MPa, for 100 µl, 150 µl, and 200 µl of PDMS, respectively. When the rotation speed was 2000 rpm, Young's modulus was 26.08 MPa, 19.2 MPa, and 9.51 MPa, respectively. The elongation at break was 3.3 %, 2.7 %, and 2.2 %, respectively. The tensile strength was 6.5 MPa, 3.2 MPa, and 3.1 MPa, respectively. In the case of samples with a spin speed of 2500 rpm, the elongation at break was 6.1 %, 3.2 %, and 3.1 %. The Young Modulus was 8.7 MPa, 6.5 MPa, and 4.1 MPa. Moreover, the tensile strength was 2.8 MPa, 0.6 MPa, and 0.2 MPa, for 100 µl, 150 µl, and 200 µl of PDMS, respectively. The mechanical testing revealed that the AM/PDMS fabricated with1500/100 (rpm/µl) and 2500/200 (rpm/µl) showed the highest and lowest mechanical properties, respectively. The suture retention result is also reported in **Supplementary** Fig. 1.

The suture retention strength, the deformation at rupture and the corresponding deformation were plotted against the amount of PDMS and rotation speed to assess PDMS proportion rotation speed based on the suture retention test result. At the beginning, the suture material that introduced some noise in the data at the beginning was straightened before a force was assigned to the specimen. The suture retention strength (FS) [47], the related deformation (ds), and the deformation at rupture (dr) [20] were specified as typical data sets. In the 1500 rpm and 2000 rpm rotation speeds, when PDMS volume increased, the Fs decreased. While in 2500 rotation speed, it is the other way around; the Fs rose from 058 to 0197 when the PDMS volume increased. ds and dr increased when the PDMS concentration increased at the same rotation speed. The significant increase in mechanical behaviors of AM/PDMS bilayer membrane compared with AM and PDMS is clearly seen in Fig. 4 (B). As can be seen, the bilayer membrane remained straight and flat when picked up by forceps, while AM was completely crumpled, both in wet forms. According to the results obtained from the cross-section view under SEM, thickness, uniformity of bilayer membrane, and mechanical behaviors, the AM/PDMS prepared by 1500 rpm and 150 µl (AM/PDMS 1500/150) was considered as our optimized ultrathin bilayer membrane, and subjected to further biological and *in vivo* implantation investigations.

3.2.3. *Water contact angle*

The results obtained from the water contact angle of AM, PDMS, and AM/PDMS 1500/150 surfaces are shown in Fig. 4(C). AM showed a WCA of 81°, and the PDMS had a hydrophobic surface showing a WCA of approximately 102°. It was revealed that by the combination of AM and PDMS, the WCA of PDMS decreased to 86°.

3.2.4. *Transparency*

The transparency of AM, PDMS and AM/PDMS 1500/150 in both dry and wet forms is shown in Fig. 4(D). It was observable that both dry and wet bilayer scaffolds are transparent membranes. Dry AM/PDMS samples seemed even more transparent than dry AM alone, as shown in Fig. 4(D).

3.2.5. *Degradation rate (weight loss%)*

The *in vitro* degradation rate ***(weight loss%)*** of AM, PDMS, and AM/PDMS bilayer scaffolds after 25 consecutive days embedding in PBS was evaluated by the observation of their surface and cross-sectional morphology with SEM (Fig. 5A) and weight loss percentage (Fig. 5B). The surface morphology of AM under SEM confirmed the morphological changes of AM during the degradation periods of 1, 7, and 14 days, while PDMS showed no sign of morphological degradation. Observation of cross-sectional view under SEM revealed that AM and AM/PDMS had around 14.74 µm, 4.54 µm, 2 µm thickness, and 12 µm, 11.83 µm, 5.17 µm thickness, after 1, 7 and 14 days embedding in PBS, respectively. Fig. 5(B) showed that degradation of PDMS and AM/PDMS layer hardly occurs in the PBS medium alone, but the AM layer lost more than 60 % of its weight in 25 days.

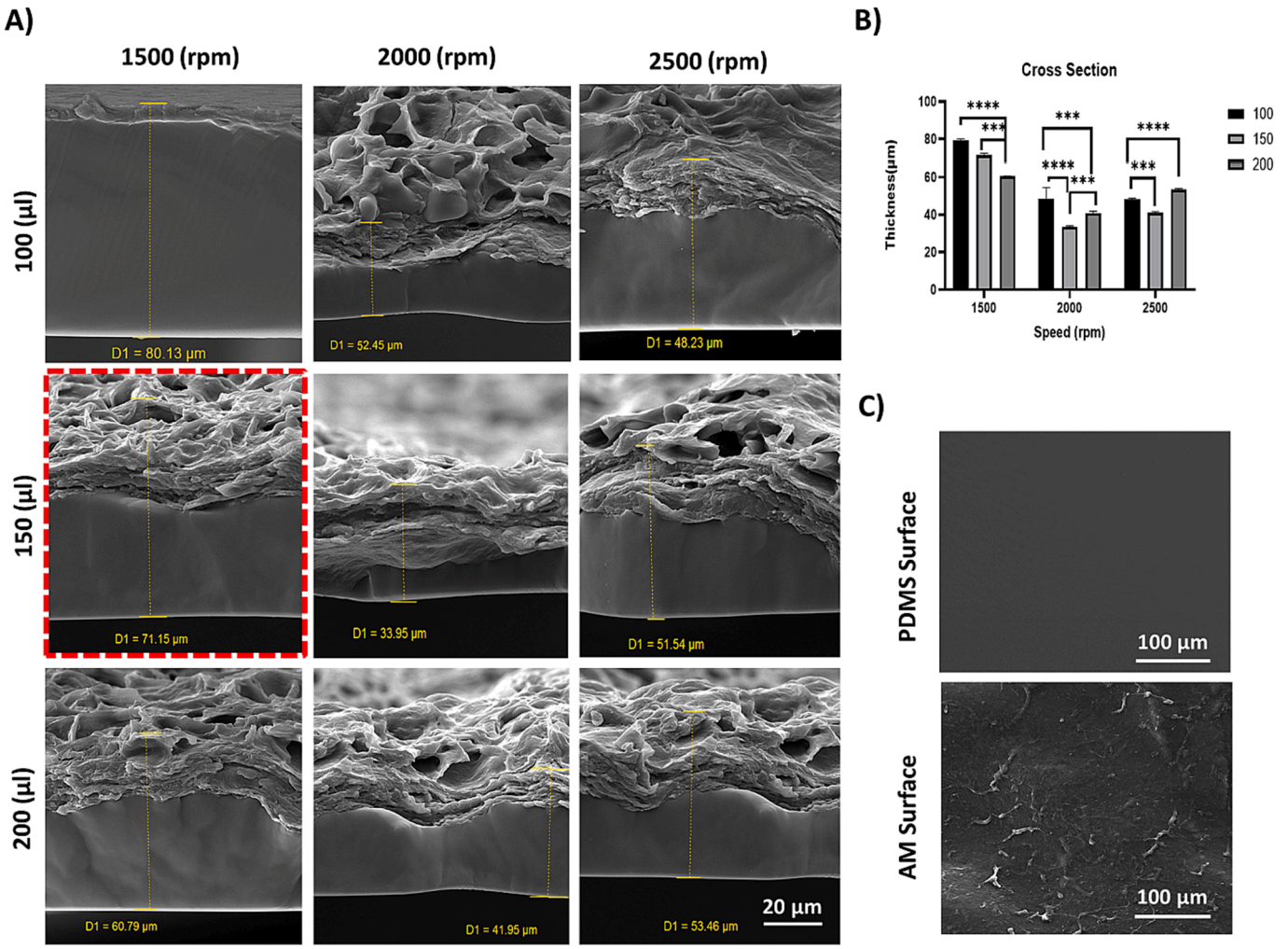

Fig. 3. Morphology of the scaffolds. (A): the cross-sectional SEM images of (AM and PDMS layers) fabricated by 100, 150, and 200 µl silicone volume and 1500, 2000, and 2500 rpm rotation speed of spinning, respectively. **(B)**: Scaffolds diameter distribution in different volumes of silicone and rotation speed. **(C)**: SEM micrograph of silicone surface and AM surface (down) of AM/PDMS scaffold. **** and *** indicate < 0.0001 and $p = 0.0008$, respectively.

3.2.6. Cell-membrane interaction behaviors

As shown in Fig. 6(A), SEM results revealed that the cells attached well to both AM and PDMS surfaces. Also, the corneal epithelial cells were expanded on both surfaces and created spindle morphology during 3 days of incubation. As can be seen, the morphology of cells on both surfaces was similar, and the physicochemical characteristics of scaffolds support cell attachments. DAPI staining was also used to examine the attachment and distribution of corneal epithelial cells on the bilayer membrane scaffold (Fig. 6B**)**. In this study, the viability and cytotoxicity properties of corneal epithelial cells cultured on the samples were determined using MTT assay. The results of the viability analysis (Fig. 6C) showed significant differences between the AM, PDMS, and AM/PDMS groups with control sample after 72 h. AM/PDMS sample significantly increased the cell viability compared with other groups. All the samples showed *in vitro* cyto-biocompatibility and supported the cellular properties as well.

3.2.7. Antibacterial properties

According to Fig. 7(A), there was no inhibition zones around the AM and AM/PDMS scaffolds for *A. bumannii*. SEM images but showed (Fig. 7B) no signs of bacteria neither on AM nor on PDMS sides of the bilayer scaffold.

3.2.8. Biocompatibility

The biocompatibility of the scaffolds was evaluated in an animal model. The scaffolds were subcutaneously implanted, and the histologic analysis and macroscopic images on days 7 and 21 post-implantation are shown in Fig. 7**(C and D)**. The subcutaneous implantation of the scaffolds in the mouse model revealed no severe inflammation at the implantation site during 21 days follow-up in both AM and AM/PDMS groups. Furthermore, macroscopic images of the implanted sites and H&E-stained slides showed no evidence of extreme acute inflammatory response in all samples on days 7 and 21 post-implantation.

3.2.9. In vivo evaluations

The optimized AM/PDMS membranes were implanted in a rabbit corneal defect model. The corneal wound healing was evaluated by macroscopic observations, histological and molecular analyses and the results compared with those wounds treated with AM and no treated wounds.

3.2.9.1. Macroscopic observations. Ethanol-induced corneal defect was used as a model for corneal defect in rabbit's eyes. When exposed to 30 % ethanol and scraped, typical signs of the corneal defect including conjunctive congestion and epithelial damage appeared. The days after transplantation, the corneal epithelium was stained with fluorescein to examine its regeneration. During the first few weeks following the operation, inflammation of the anterior segment, including swelling of the soft tissues and dense white exudation, were developed. After the

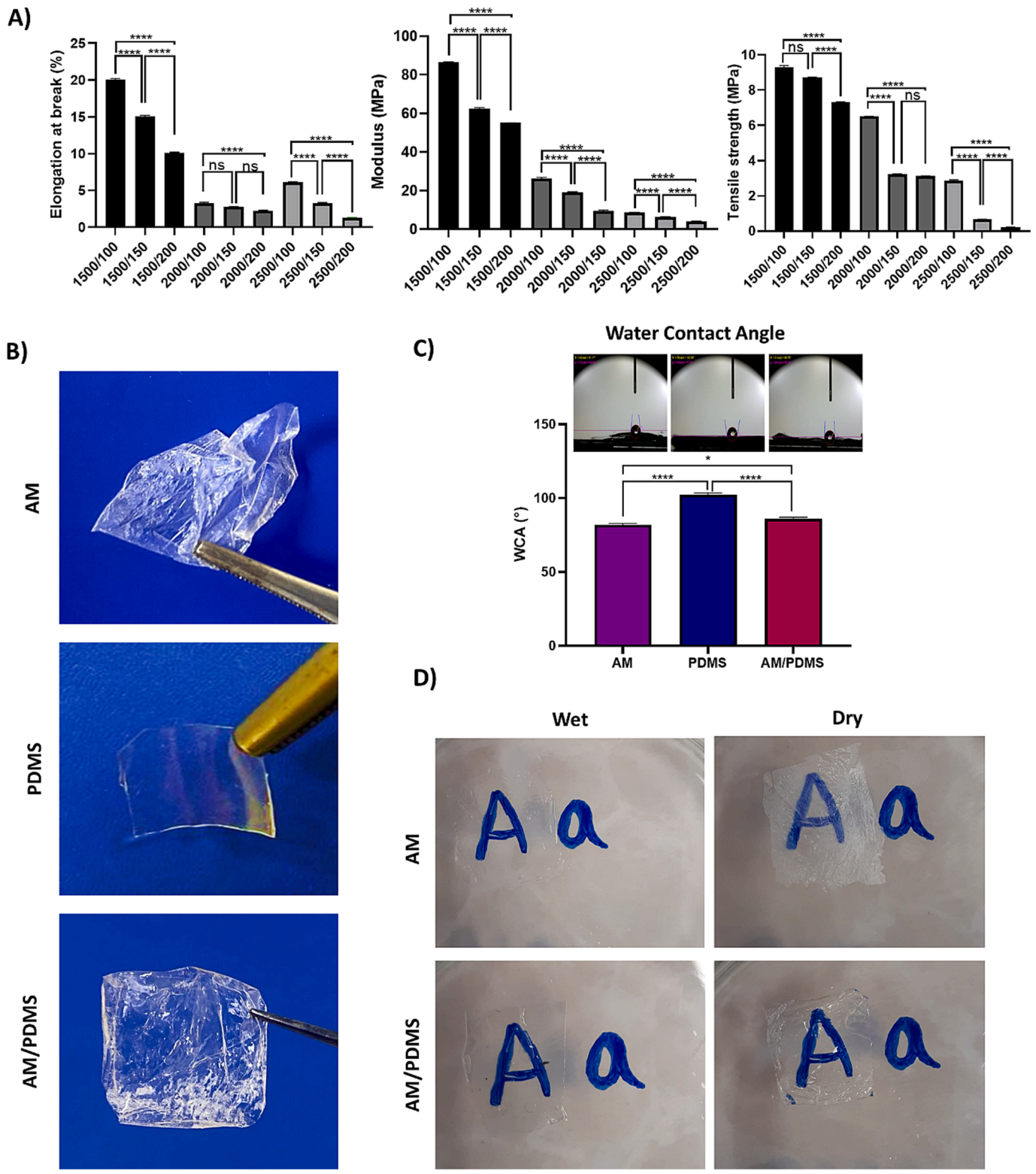

Fig. 4. (A): Mechanical properties. Elongation at break (%), Young's modulus (MPa), and tensile strength (MPa) (N = 3). Tensile strength and elastic modulus were under the influence of both PDMS volume and rotation speed. **(B): Macroscopic image of membranes**. Macroscopic images of Wet AM (top), wet PDMS (middle), and wet AM/PDMS 1500/150 bilayer scaffold (down). **(C): Water contact angle (WCA) measurements**. Images of a water droplet on AM, PDMS, and AM/PDMS surfaces. **(D): Transparency of scaffolds**. AM and AM/PDMS transparency in both wet and dry states. * and **** indicate $P \leq 0.05$ and $p = 0.0001$, respectively.

second week, exudation disappeared, and limbus neovascularization indicated chronic inflammation. Corneal transparency improved in the AM/PDMS composite membrane group, and neovascularization was significantly reduced. Conversely, the conjunctive epithelium gradually covered the corneal defect in the AM group, which also resulted in cloudy corneas with extensive neovascularization (Fig. 8A).

3.2.9.2. H&E staining. On day 21 post-injury, the corneal defect tissues

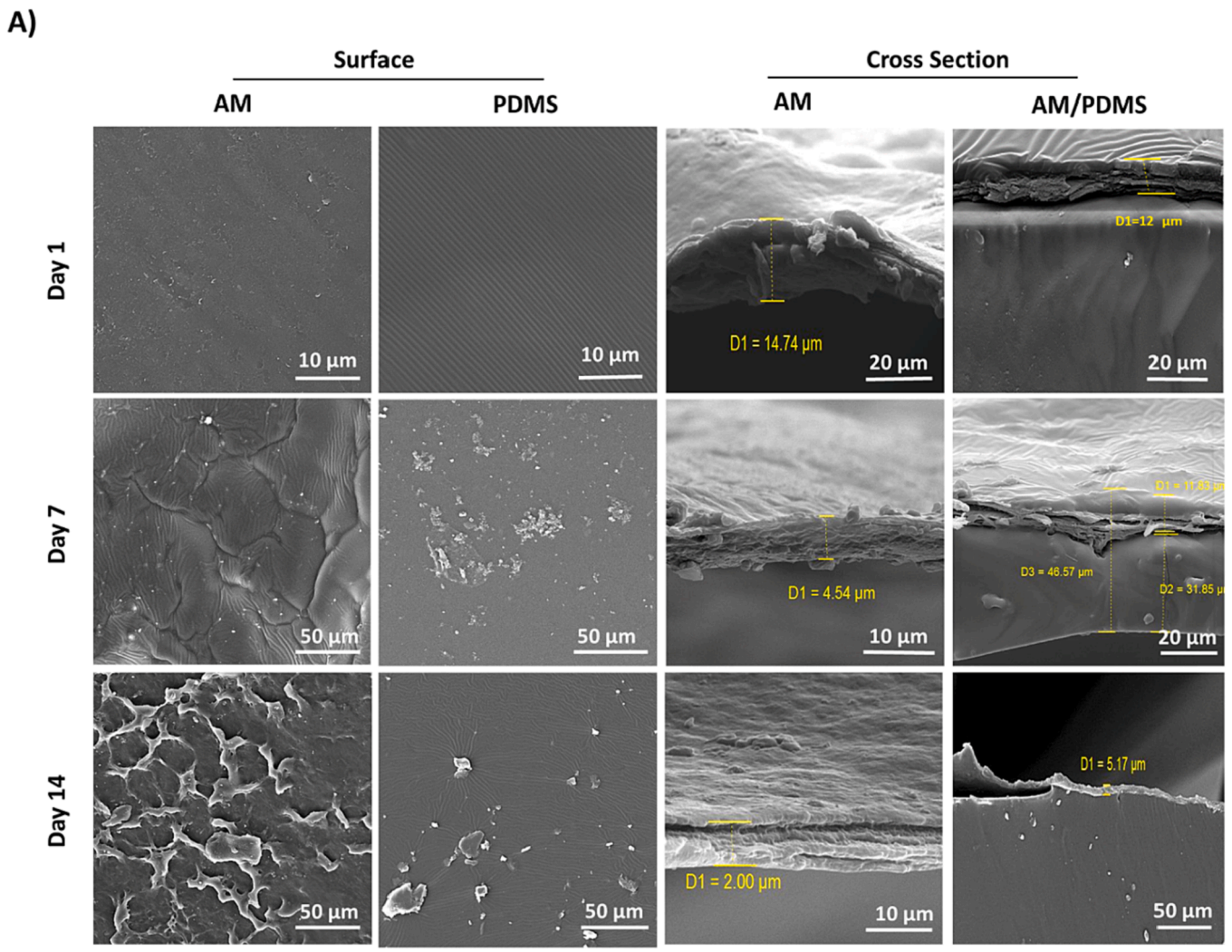

Fig. 5. In vitro biodegradation. (A): SEM micrographs of both surface and cross-section of AM and AM/PDMS at days 7 and 14 of incubation in PBS solution. **(B)**: The weight loss (%) of the prepared samples in the PBS solution for 25 consecutive days.

were collected and stained with H&E. H&E staining results at week 3 revealed that the cornea's epithelial morphology and hierarchy had been restored. In particular, the polygonal pterygium, the upper basal cells, and the superficial flat cells resembled normal corneal epithelium. Contrary to the treated wound, epithelial cells in the control wounds were fusiform, bulky, or polygonal with a loose connection. Additionally, in the control group, the cells were irregularly arranged, and goblet-like cells were clearly visible. As shown in Fig. 8(B), H&E staining demonstrated that the AM/PDMS group had better epithelial delaminated cell morphology. The composite membrane group had similar corneal stromal collagen content compared with the standard control group (normal cornea with no defect).

3.2.9.3. Masson's trichrome. Fig. 8(C) shows the MT staining images. At day 21 of treatment, collagen synthesis and deposition significantly decreased in the AM and AM/PDMS experimental groups when

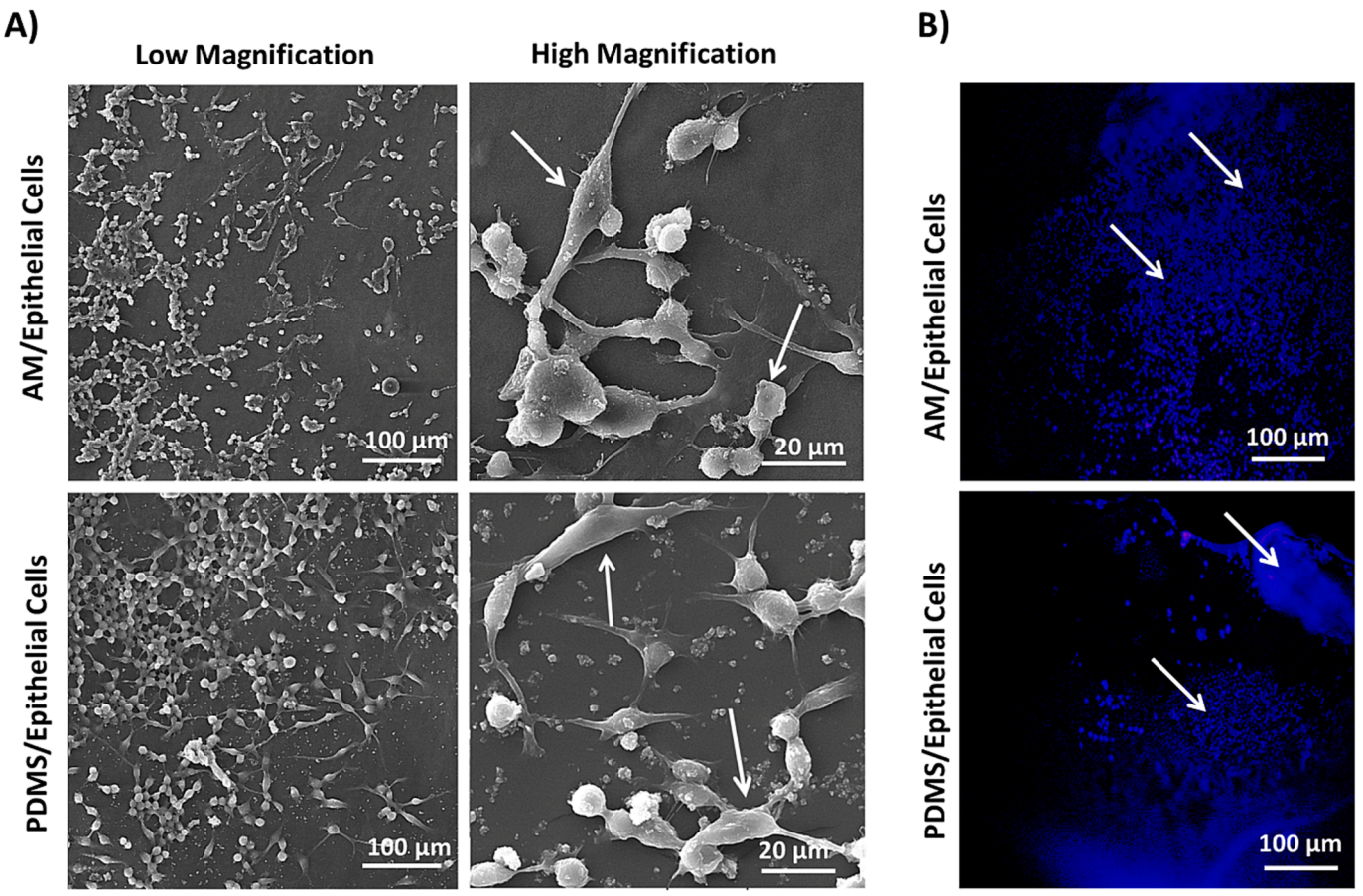

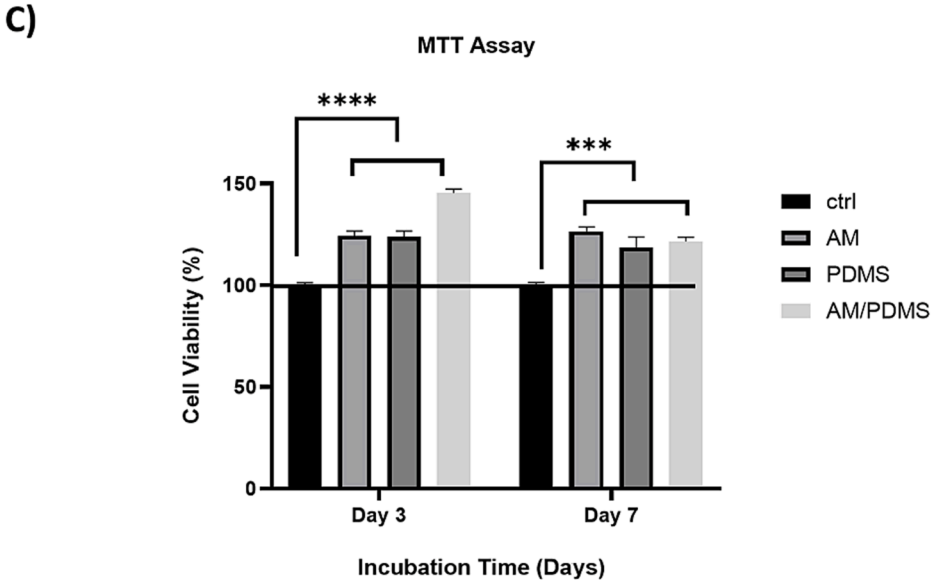

Fig. 6. Cell-membrane interaction behavior. **(A)**: SEM micrographs of the human corneal epithelial cells cultured on AM (top) and PDMS (down) surfaces of bilayer scaffolds after 3 days at low and high magnification. **(B)**: Typical DAPI staining of samples. "Top" human corneal epithelial cells on AM surface and "down" human corneal epithelial cells on PDMS surface of AM/PDMS scaffold. White arrows indicate cells in (A) and (B) figures. **(C)**: cytotoxicity and cell viability of AM, PDMA, and AM/PDMS scaffold were determined by MTT assay for 3 and 7 days after incubation time. Non-treated cells were considered as the positive control. (Independent sample *t*-test, $P < 0.05$).

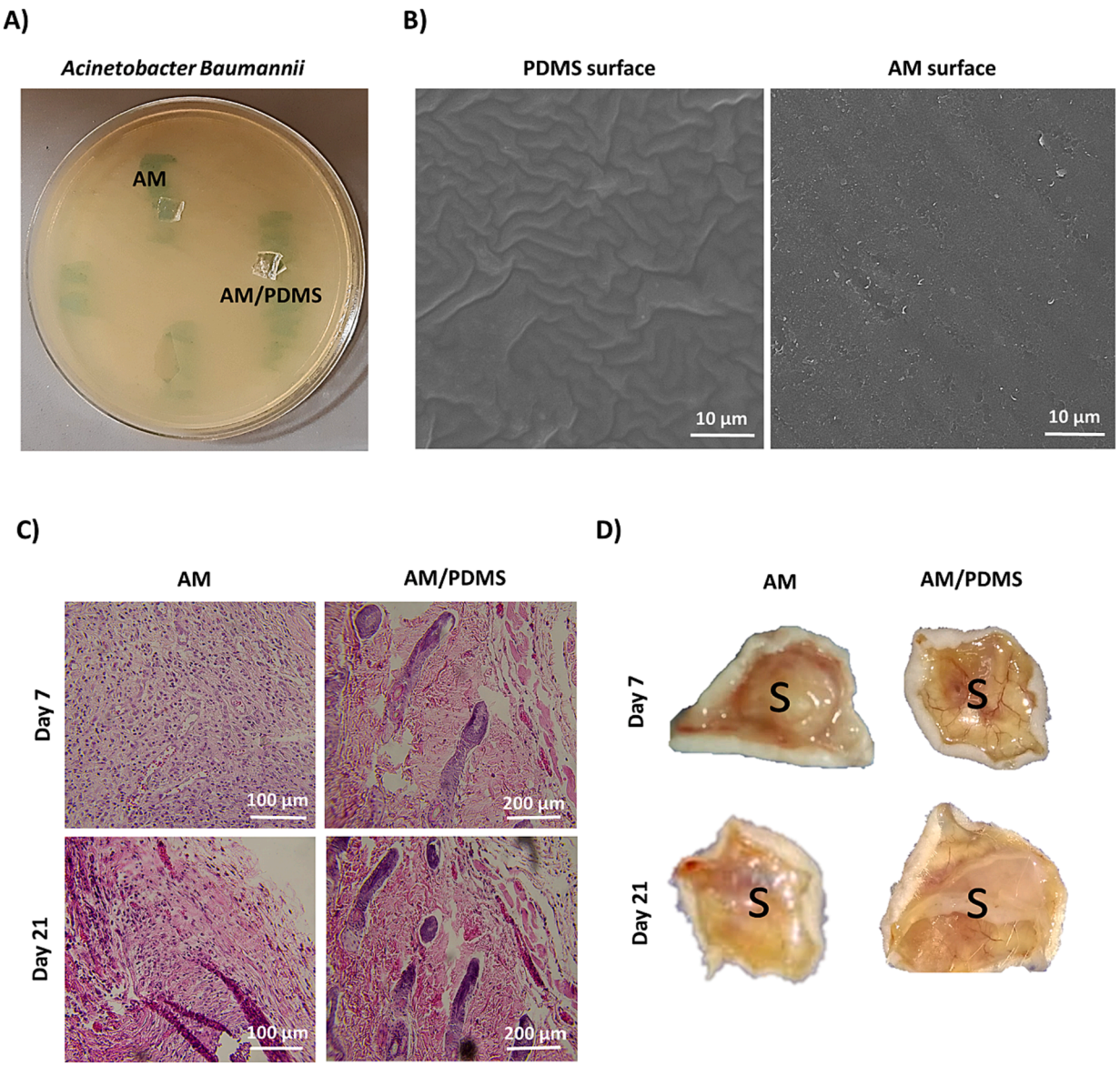

Fig. 7. (A): Antibacterial behavior; disk diffusion test. Antibacterial behavior of AM and AM/PDMS against *Acinetobacter baumannii*. The bacterial growth inhibition zones were not observed for both AM and AM/PDMS. **(B): SEM micrographs**. SEM micrographs indicated no signs of bacteria, neither on AM nor on the PDMS surface of the bilayer scaffold. **(C, D): An analysis of subcutaneously implanted scaffolds.** The histologic analysis of AM and AM/PDMS scaffolds on days 7 and 21 post-implantation with H&E staining (left) and the macroscopic analysis of AM and AM/PDMS on days 7 and 21 post-implantation (right). S indicated scaffold.

compared with a corneal defect with no treatment. The collagen bundles in the corneal defect with no treatment (control) were mainly aligned, whereas the collagen bundles in the wound bed treated with AM and AM/PDMS were arranged in a basket weave pattern.

3.2.9.4. Gene expression. The RT-PCR results are presented in Fig. 8(D). COL1A1 and TGF-β1 expression was significantly reduced in AM and AM/PDMS compared with control. MMP-9 showed a statistically down-regulation in the wounds implanted compared with those corneal defect treated with AM and no treatment (control). Both AM and AM/PDMS groups had a significant increase in MMP-9 when compared with the control. The evaluation of pro-inflammatory gene expression revealed significant down-regulations in the expression of TNF-α and IL-6 in both AM and AM/PDMS in comparison with control wounds. No significant change in the relative expression of VEGFa was observed between all the experimental groups.

4. Discussion

In this study, an amniotic membrane was coated with a very thin layer of PDMS to develop an ultrathin bilayer membrane with improved mechanical and biological attributes suitable for corneal wound healing application. To analyze the improvement of AM, cell attachment and biocompatibility, biodegradability, tensile and suture retention strength of the composition were measured and compared with conventional AM characteristics. PDMS is a polymer with good elastomeric properties, biocompatibility, gas permeability, transparency and therefore commonly used in biomedical applications [21]. Indeed, PDMS has previously been used to improve the biomechanical, biocompatibility and stickiness properties of hydrogels for wound dressings [48]. As mentioned before, AM is a biomaterial that is widely used as scaffolds and wound dressings due to its biocompatibility, transparency, anti-fibrotic, anti-inflammatory and, ECM basement structure and lack of immunogenicity. However, the disadvantage of this membrane is its

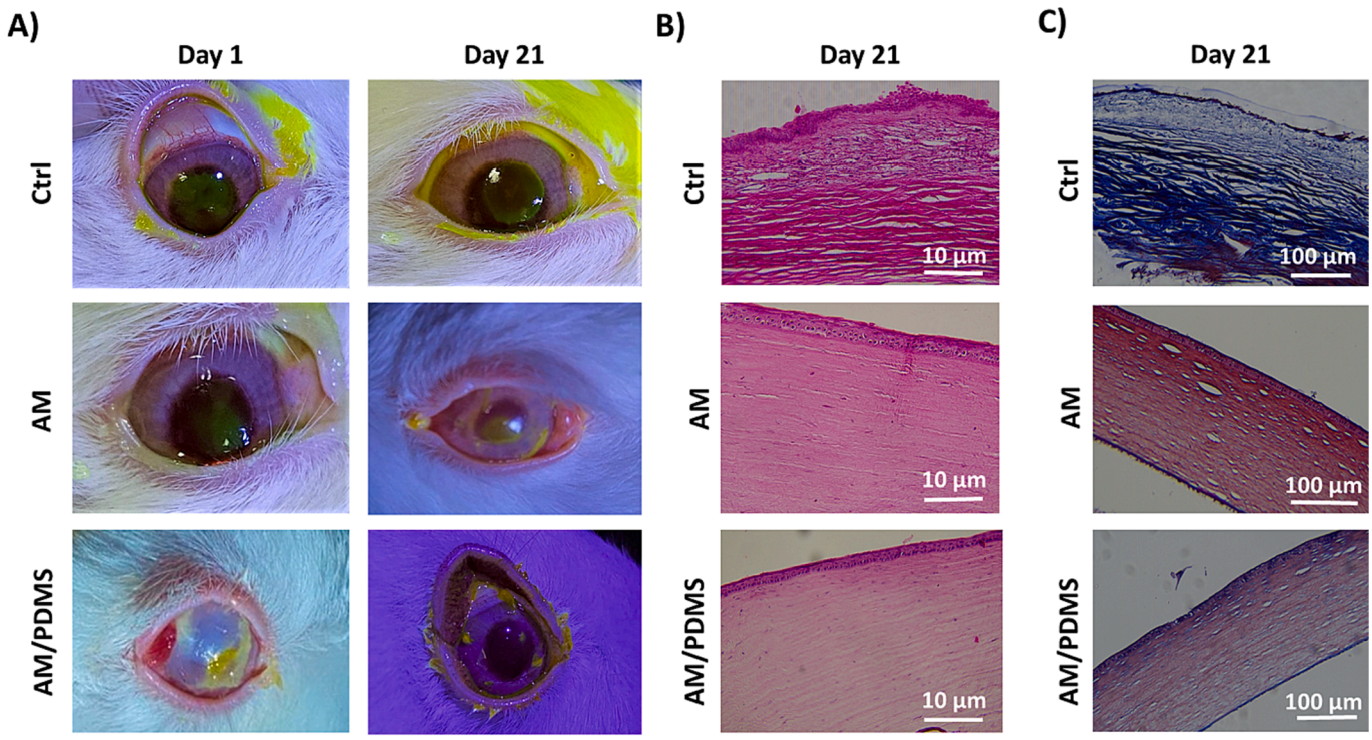

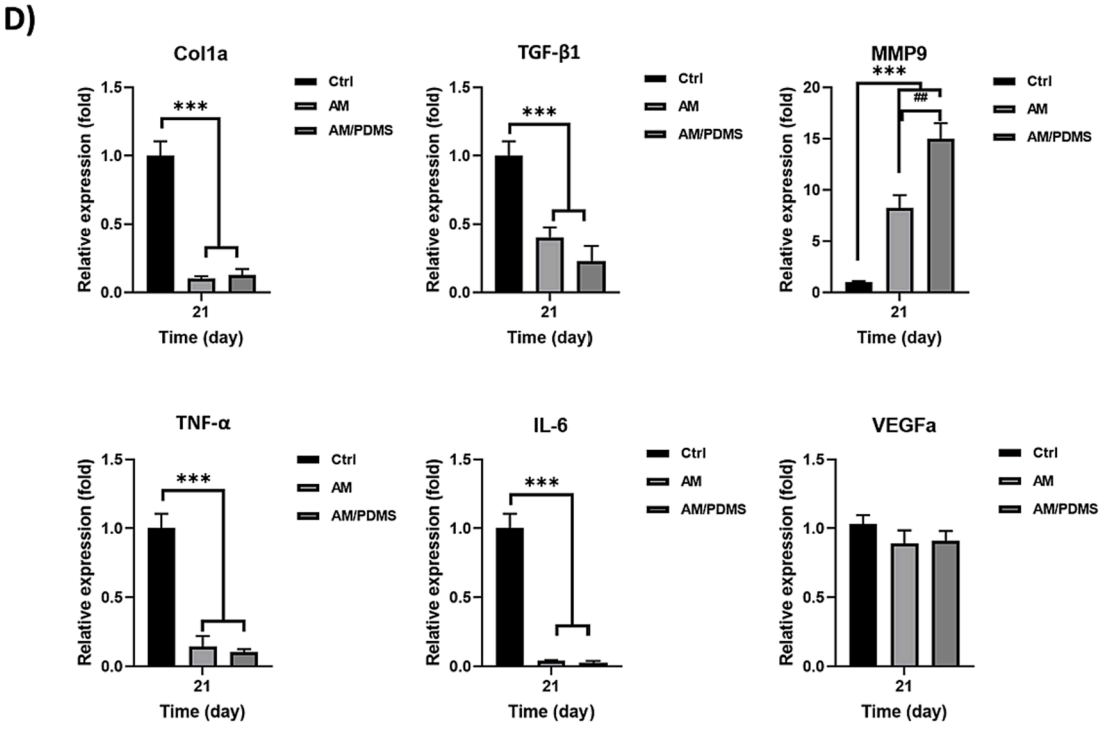

Fig. 8. (A): Macroscopic observation of cornea. The surgery results and macroscopic images of AM and AM/PDMS implantation on the 21st day after defect under fluorescein staining by the camera. The left eye and right eye served as a control and treated groups, respectively. Serial images of the same cornea implanted with AM/PDMS scaffold indicated a significant reduction in corneal haze compared with AM and the control group. **(B): Corneal H&E staining**. **H&E staining**, 21 days after AM and AM/PDMS scaffold transplantation. The AM/PDMS group had better epithelial stratified cell morphology than the AM and control groups. **(C): Masson's Trichrome (MT) staining**. Masson's Trichrome (MT) stained sections on day 21 post-operation that indicate the collagen bundles in the wound bed treated with AM and AM/PDMS were arranged in a basket weave pattern, whereas in the control group were mainly aligned. **(D): Gene expression evaluation**. Comparison of relative gene expression (fold) between the experimental groups of Ctrl (Control), AM (Amniotic membrane), and AM/PDMS (bilayer membrane). *** And ## indicated significant difference with control ($P < 0.001$) and AM ($p < 0.01$), respectively.

poor biomechanical properties. This in turn makes it difficult to handle and suture on the wound-site [47]. For this purpose, the amniotic membrane was decellularized and characterized by H&E and DAPI staining. The decellularized AMs were then coated with various volumes of PDMS at three different spinning speeds in nine different experimental groups. The SEM micrographs from surface and cross-sectional view of the bilayer membranes revealed that the PDMS were almost uniformly coated over AM in all the groups with thicknesses ranging between 33 and 80 μm. The AM coated with 150 μl PDMS at 2000 rpm was the thinnest bilayer membrane with a thickness of about 33.95 μm. It was expected that with increasing the speed of rotation, the thickness would decrease however, SEM data showed that in 150 μl and 200 μl volumes of PDMS when the speed changed from 2000 to 2500 rpm, the thickness of the bilayer scaffold was increased. It might be due to the viscosity of PDMS at a higher volume, even at higher speed, the larger volumes could not be sufficiently dispersed to coat the AM. Tensile strength and suture retention showed the highest strength (9 MPa and 0.6 N respectively), for the groups made from 100 μl PDMS at 1500 rpm rotation speed. The mechanical data confirmed that in the lower speed of rotation (1500 rpm), the mechanical strength had been upper than the others, and the lowest mechanical strength belonged to the speed of 2500 rpm groups (0.5–3 MPa). The data clearly showed that the thicker bilayer membranes showed higher mechanical properties. Therefore, the mechanical data confirmed the SEM images of the groups. The bilayer membrane with lowest thickness and highest mechanical property (150 μl PDMS and 1500 rpm) was considered as the best composition for our purpose and therefore subjected to further *in vitro* and *in vivo* evaluations. Furthermore, our macroscopic observations clearly confirmed a significant improvement in the mechanical properties of the AM/PDMS composition, which make it easier to handle, when compared with AM alone. Some attempts have been made to engineer AM-based scaffolds with improved mechanical properties using cross-linking agent and various biomaterials [19,49–51]. Several studies have used crosslinking materials such as carbodiimide, genipin and glutaraldehyde to improve the mechanical strength and decrease biodegradation rate of AM [50,52,53]. Although these chemical cross-linkers seem safe, they could be toxic and thereby decrease biocompatibility. In a previous study from our end [54], the decellularized AM was electrospun with silk fibroin protein to fabricate a 3-D bi-layered scaffold with improved biomechanical properties. The AM/ESF displayed a thickness of 127 μm and a suture retention strength corresponding to 0.6 N – both which were better than AM alone. The application of synthetic materials such as polycaprolactone (PCL) to improve the biomechanical properties of AM has also been explored [55]. For instance, Hadipour *et al.*[55] showed that the tensile strength of AM/PCL composite (0.41 MPa) significantly increased compared with AM (0.16 MPa), while simultaneously enhance the degradation rate over a two week period. PDMS is a hydrophobic materials due to its CH_3 groups on the surface and making it hard to wet with aqueous solutions[20,23]. As expected, the data obtained from contact angle revealed that coating with PDMS decreased the wettability, as AM/PDMS and AM had 86° and 81° contact angel values, respectively. Some other AM composite scaffolds such as electrospun PLGA fibers on AM showed an increase in the surface hydrophobicity as well [56]. Degradation levels of AM/PDMS and AM were evaluated by weighting, and observing scaffold surface and cross-sections during 25 consecutive degradation days incubation in PBS. Degradation assay revealed that the AM was mostly degraded (up to 60 %) after 25 consecutive day's incubation in PBS The SEM images of the surface and cross-sections of AM/PDMS represented a reduction in thickness (~5.17 μm) and degradation of the AM surface of bilayer scaffold, when compared with AM alone (~2 μm). Indeed, coating AM with PDMS caused less exposure of AM surface with PBS solution, and slowed down the degradation rate. Rapid degradation of AM is a disadvantage for our applications and needs to be circumvented. AM has a high degradation rate on the exposure of the PBS and lysozyme that was reported in studies (about 80 % in 6 days) [51]. Along these lines, our findings confirmed that the addition of PDMS layer significantly prolonged the biodegradability of AM. Previous studies have also showed that composites such as PCL (45) and silk fibroin (48) with AM could slow the biodegradation rate of AM. Their experiment showed, that AM degraded completely after two weeks compared with the AM/Silk which degraded by 40 % in PBS. Furthermore, AM and PCL/AM degraded by 80 % and 50 % respectively after 6 days in PBS. These AM composites caused delays in the fast degradation profile of AM. Indeed, it seems likely that the differences in the degradation rates of AM in the studies could be due to the primary thickness of cellular AM or its different decellularization processes. AM is a transparent membrane, which makes it possible to see the wounds behind the implanted AM for monitoring wound healing, necrosis and infection during post-implantation follow-up (51). Some studies have shown that cross-linked AM had a better light transmittance in wet condition [47]. PDMS had an excellent optical transparency at room temperature and it could be changed due to the heating processes[57,58]. Our observations showed that both AM and AM/PDMS were transparent in dry form. In the wet form, however, the bilayer scaffold showed more transparency than AM. A possible discussion is that the AM is laminated with PDMS. Previous studies confirmed the cyto-compatibility and cell adhesion properties of both AM and PDMS [54,59,60]. In our study, the cyto-biocompatibility of AM and AM/PDMS was evaluated for limbal epithelial cells. The cells were cultured on both AM and AM/PDMS scaffold and examined for cell-membrane morphology under SEM and MTT assay. The SEM micrographs showed that the cells were well attached on both sides of the scaffolds. MTT assay on days 3 and 7 exposure of the cells with membranes confirmed the cyto-biocompatibility of AM and AM/PDMS, when compared with the cells in culture plate without scaffold. The cells cultured on the AM/PDMS showed slightly increased viability compared with AM and control group on day 3, but no significant change in cell viability value was observed on day 7. This may be due to the effect of the improved mechanical properties on cell behavior in accordance with recent studies [61,62]. Furthermore, DAPI staining confirmed the distribution of limbal epithelial cells on AM and AM/PDMS surfaces. All these data showed that both AM and AM/PDMS had excellent cell adhesion properties and were completely cyto-biocompatible. The antibacterial activity of AM was proved in previous studies [63–65], and one showed that AM could not kill some resistant strains of bacteria [19,64,65]. On the other hand, the antibacterial property of AM depends on the type of bacteria and the time of preservation and quality of AM [19,66]. Disc diffusion assay *(A. bumannii* ATCC 19606) on AM and AM/PDMS showed no inhibition zone of bacterial growth formed around the membranes. SEM micrographs showed no bacteria attached on both surfaces of membrane. *A baumannii* is considered as the most often responsible for ocular defect infections [67,68]. Histological observations of AM and AM/PDMS after subcutaneous implantation during 7 and 21 days indicated no signs of acute inflammation and graft rejection. Our results confirmed the *in vivo* biocompatibility of both AM and AM/PDMS, which was consistent with other relevant studies [69,70]. Generally speaking, AM membranes has been considered as an excellent dressing and temporary graft for management of corneal wound defects [63,71]. In our study, the potential of the optimized AM/PDMS on cornea healing was determined after applying to corneal wounds created in a rabbit animal model. In this direction the healing rate was compared with those wounds dressed with AM and untreated wounds. The macroscopic observations using fluorescein and H&E staining indicated that the wounds dressed with AM and AM/PDMS had completely healed at day 21 post-surgery. We showed the degradation rate (weight loss%) of scaffold is very slow during 21 days *in vitro*. However, it completely disappeared after 21 days post- implantation *in vivo*. In this study, the *in vitro* degradation in PBS measures the weight loss (%), and is completely different with enzymatic biodegradation. After implantation *in vivo*, the scaffold is exposed to a wide range of enzymatic degradation processes, and as expected, the biodegradation of scaffolds *in vivo* is very faster than

degradation rate (weight loss%) in PBS *in vitro*. Furthermore, observations showed that the cornea surface in the treated groups was completely transparent and with no signs of inflammation after 21 days. Besides, H&E staining demonstrated that in the control wounds (no treatment), the epithelium was thick and not formed entirely with inflammatory cells being present in the injury site. On the other hand, in AM and AM/PDMS groups, a complete re-epithelization and uniform epithelium layer was observed. Finally, RT-PCR revealed diminished expression levels of COL1A1, TGF-β1, TNF-α, and IL-6 in AM and AM/PDMS groups in comparison with the control group. According to previous studies, these genes are related to collagen, myo-fibroblast, and scar formation or inflammation, respectively [72,73]. In contrast, the MMP-9 expression level in AM and AM/PDMS was significantly upper than in the non-treated groups. Matrix metalloproteinase-9 (MMP9) can affect the basal epithelial cells migration, and promote the remodeling of sub-epithelial basement membrane and wound healing by degradation of the extracellular matrix [74,75]. Also, implantation of corneal defects with both AM and AM/PDMS slightly decreased the VEGF-A expression in defect site, indicating less new angiogenesis during healing. This result may be due to the suppression role of anti-inflammatory agents [74]. On the other hand, decrease in angiogenesis of corneal defect during healing positively affect the high quality wound healing in cornea [76].

5. Conclusion

Amniotic membrane as a biological scaffold with attractive attributes has been used in tissue engineering and for wound dressings for many years. Especially in corneal defect healing. Besides its extraordinary characteristic such as biocompatibility, safety, and anti-inflammatory, the use of AM is still challenging because of its weak biomechanical properties. In this study, we covered AM with a very thick layer of PDMS, which is known as a transparent, biocompatible, firm, and stable biomaterials, to improve the AM biomechanical weaknesses, and thereby develop an optimized ultrathin and transparent bilayer scaffold for biomedicine utilizations. *In vitro* characterizations and observations showed that AM/PDMS bilayer scaffold was ultrathin (about 40–80 μm), suturable with improved in biomechanical characteristics (mechanical strength, degradation, and transparency) compared with AM. Cellular examinations indicated that epithelial cells were well attached to the AM/PDMS scaffold, while *in vivo* studies in a rabbit cornea model showed complete healing of epithelial defects. Altogether, our study suggest that AM/PDMS is an excellent dressing for corneal tissue injuries, and maybe even for other dressing applications.

Author contribution

MG conceived and designed the study. ZE, ZND, SA, JM, HC, SHD, MK, MNB, HGH, AA, AH and M Ghaffari performed the experiments. MG, ZE, ZND, SA, JM and AH analyzed the data and interpreted the results. ZE, ZND, SA, JM, HC and MG prepared the manuscript. MG, ADP, ZE, ZND, HN and MG reviewed during the manuscript preparation and revised the manuscript.

CRediT authorship contribution statement

Zahra Esmaeili: Writing – original draft, Methodology, Investigation, Formal analysis. **Zeinab Nokhbehdehghan:** Writing – review & editing, Writing – original draft, Methodology, Investigation, Formal analysis. **Sanaz Alizadeh:** Writing – original draft, Visualization, Methodology, Investigation, Formal analysis. **Jila majidi:** Writing – original draft, Visualization, Investigation, Formal analysis. **Hadi Chahsetareh:** Methodology, Investigation, Formal analysis. **Seyed-Hashem Daryabari:** Visualization, Investigation. **Maryam Nazm-Bojnourdi:** Methodology, Investigation. **Majid Kadkhodaie:** Visualization, Methodology, Investigation. **Maryam Ghaffari:** Methodology, Investigation. **Ali Hashemi:** Methodology, Investigation, Formal analysis. **Hatef Ghasemi Hamidabadi:** Methodology, Investigation. **Ahmad Ahmadzadeh Amiri:** Methodology, Investigation. **Hajar Nasiri:** Writing – review & editing. **Alireza Dolatshahi-Pirouz:** Writing – review & editing. **Mazaher Gholipourmalekabadi:** .

Declaration of competing interest

The authors declare that they have no known competing financial interests or personal relationships that could have appeared to influence the work reported in this paper.

Data availability

Data will be made available on request.

Acknowledgment

This study was funded by a grant from the Mazandaran University of Medical Sciences under grant number 17206.

Appendix A. Supplementary data

Supplementary data to this article can be found online at https://doi.org/10.1016/j.matdes.2023.112614.

References

[1] B. Barrientez, S.E. Nicholas, A. Whelchel, R. Sharif, J. Hjortdal, D. Karamichos, Corneal injury: Clinical and molecular aspects, Exp. Eye Res. 186 (2019) 107709.
[2] C.E. Ghezzi, J. Rnjak-Kovacina, D.L. Kaplan, Corneal tissue engineering: recent advances and future perspectives, Tissue Eng. B Rev. 21 (3) (2015) 278–287.
[3] B. Kong, S. Mi, Electrospun scaffolds for corneal tissue engineering: A review, Materials 9 (8) (2016) 614.
[4] D.W. DelMonte, T. Kim, Anatomy and physiology of the cornea, J Cataract Refract Surg 37 (3) (2011) 588–598.
[5] D. Willmann, L. Fu, S.W. Melanson, Corneal injury, StatPearls [Internet], StatPearls Publishing, 2021.
[6] U. Vaidyanathan, G.C. Hopping, H.Y. Liu, A.N. Somani, Y.C. Ronquillo, P. C. Hoopes, M. Moshirfar, Persistent corneal epithelial defects: a review article, Medical Hypothesis, Discov. Innovat. Ophthalmol. 8 (3) (2019) 163.
[7] B. Wirostko, M. Rafii, D.A. Sullivan, J. Morelli, J. Ding, Novel therapy to treat corneal epithelial defects: a hypothesis with growth hormone, Ocul. Surf. 13 (3) (2015) 204–212, e1.
[8] N. Wu, D. Gong, J. Chen, L. Chen, H. Sun, Y. Fu, Design of functional decellularized matrix for conjunctival epithelial stem cell maintenance and ocular surface reconstruction, Mater. Des. 224 (2022) 111278.
[9] D. Yan, F. Yu, D. Gong, S. Zhang, H. Sun, Y. Fu, Cell-free matrix derived from adipose mesenchymal stromal cells enhances corneal rehabilitation via delivery of nerve regenerative PGRN, Mater. Des. 227 (2023) 111786.
[10] B.H. Jeng, Treating the nonhealing epithelial defect.
[11] L.R. Katzman, B.H. Jeng, Management strategies for persistent epithelial defects of the cornea, Saudi J. Ophthalmol. 28 (3) (2014) 168–172.
[12] Q. Gong, Y. Zhao, T. Qian, H. Wang, Z. Li, Functionalized hydrogels in ophthalmic applications: Ocular inflammation, corneal injuries, vitreous substitutes and intravitreal injection, Mater. Des. 111277 (2022).
[13] R.N. Palchesko, S.D. Carrasquilla, A.W. Feinberg, Natural biomaterials for corneal tissue engineering, repair, and regeneration, Adv. Healthc. Mater. 7 (16) (2018) 1701434.
[14] A. Vlasov, R.K. Sia, D.S. Ryan, M.J. Mines, R.D. Stutzman, B.A. Rivers, S.C. Tseng, K.S. Bower, Sutureless cryopreserved amniotic membrane graft and wound healing after photorefractive keratectomy, J. Cataract. Refract. Surg. 42 (3) (2016) 435–443.
[15] B. Zeng, P. Wang, L.-J. Xu, X.-Y. Li, H. Zhang, G.-G. Li, Amniotic membrane covering promotes healing of cornea epithelium and improves visual acuity after debridement for fungal keratitis, Int. J. Ophthalmol. 7 (5) (2014) 785.
[16] A. Kheirkhah, V. Casas, V.K. Raju, S.C. Tseng, Sutureless amniotic membrane transplantation for partial limbal stem cell deficiency, Am. J. Ophthalmol. 145 (5) (2008) 787–794.
[17] C.L. Allen, G. Clare, E.A. Stewart, M.J. Branch, O.D. McIntosh, M. Dadhwal, H. S. Dua, A. Hopkinson, Augmented dried versus cryopreserved amniotic membrane as an ocular surface dressing, PLoS One 8 (10) (2013) e78441.
[18] M. Bizrah, A. Yusuf, S. Ahmad, An update on chemical eye burns, Eye 33 (9) (2019) 1362–1377.
[19] M. Gholipourmalekabadi, B. Farhadihosseinabadi, M. Faraji, M.R. Nourani, How preparation and preservation procedures affect the properties of amniotic membrane? How safe are the procedures? Burns 46 (6) (2020) 1254–1271.

[20] A. Victor, J. Ribeiro, F.F. Araújo, Study of PDMS characterization and its applications in biomedicine: A review, J. Mechan. Eng. Biomechan. 4 (1) (2019) 1–9.

[21] I. Miranda, A. Souza, P. Sousa, J. Ribeiro, E.M. Castanheira, R. Lima, G. Minas, Properties and applications of PDMS for biomedical engineering: A review, J. Functl. Biomater. 13 (1) (2021) 2.

[22] M.P. Wolf, G.B. Salieb-Beugelaar, P. Hunziker, PDMS with designer functionalities—Properties, modifications strategies, and applications, Prog. Polym. Sci. 83 (2018) 97–134.

[23] M.-E. Vlachopoulou, P. Petrou, S. Kakabakos, A. Tserepi, K. Beltsios, E. Gogolides, Effect of surface nanostructuring of PDMS on wetting properties, hydrophobic recovery and protein adsorption, Microelectron. Eng. 86 (4–6) (2009) 1321–1324.

[24] C. Hassler, T. Boretius, T. Stieglitz, Polymers for neural implants, J Polym Sci B 49 (1) (2011) 18–33.

[25] M.F. Maitz, Applications of synthetic polymers in clinical medicine, Biosurf. Biotribol. 1 (3) (2015) 161–176.

[26] S. Torino, B. Corrado, M. Iodice, G. Coppola, Pdms-based microfluidic devices for cell culture, Inventions 3 (3) (2018) 65.

[27] K. Raj, M.S. Chakraborty, PDMS microfluidics: A mini review, J. Appl. Polym. Sci. 137 (27) (2020) 48958.

[28] J. Kim, E. Cha, J.U. Park, Recent advances in smart contact lenses, Adv. Mater. Technol. 5 (1) (2020) 1900728.

[29] S. Khosravimelal, M. Mobaraki, S. Eftekhari, M. Ahearne, A.M. Seifalian, M. Gholipourmalekabadi, Hydrogels as emerging materials for cornea wound healing, Small 17 (30) (2021) 2006335.

[30] P. Bhattacharjee, B.L. Cavanagh, M. Ahearne, Effect of substrate topography on the regulation of human corneal stromal cells, Colloids Surf. B Biointerfaces 190 (2020) 110971.

[31] S. Xiong, H. Gao, L. Qin, Y.-G. Jia, L. Ren, Engineering topography: Effects on corneal cell behavior and integration into corneal tissue engineering, Bioact. Mater. 4 (2019) 293–302.

[32] M. Gholipourmalekabadi, S. Khosravimelal, Z. Nokhbedehghan, M. Sameni, V. Jajarmi, A.M. Urbanska, H. Mirzaei, M. Salimi, N.P.S. Chauhan, M. Mobaraki, Modulation of hypertrophic scar formation using amniotic membrane/electrospun silk fibroin bilayer membrane in a rabbit ear model, ACS Biomater Sci. Eng. 5 (3) (2019) 1487–1496.

[33] S. Khosravimelal, M. Momeni, M. Gholipur, S.C. Kundu, M. Gholipourmalekabadi, Protocols for decellularization of human amniotic membrane, Methods Cell Biol. Elsevier (2020) 37–47.

[34] S. Jabbehdari, G. Yazdanpanah, L.N. Kanu, K.N. Anwar, X. Shen, B. Rabiee, I. Putra, M. Eslani, M.I. Rosenblatt, P. Hematti, Reproducible derivation and expansion of corneal mesenchymal stromal cells for therapeutic applications, Transl. Vis. Sci. Technol. 9 (3) (2020) 26.

[35] P. Farshi, R. Salarian, M. Rabiee, S. Alizadeh, M. Gholipourmalekabadi, S. Ahmadi, N. Rabiee, Design, preparation, and characterization of silk fibroin/carboxymethyl cellulose wound dressing for skin tissue regeneration applications, Polym. Eng. Sci. 62 (9) (2022) 2741–2749.

[36] S. Kutlehria, T.C. Dinh, A. Bagde, N. Patel, A. Gebeyehu, M. Singh, High-throughput 3D bioprinting of corneal stromal equivalents, J. Biomed. Mater. Res. Part B: Appl. Biomater. 108 (7) (2020) 2981–2994.

[37] M. Jafarkhani, A. Fazlali, F. Moztarzadeh, Z. Moztarzadeh, M. Mozafari, Fabrication and characterization of PLLA/chitosan/nano calcium phosphate scaffolds by freeze-casting technique, Ind. Eng. Chem. Res. 51 (27) (2012) 9241–9249.

[38] S. Simorgh, P.B. Milan, M. Saadatmand, Z. Bagher, M. Gholipourmalekabadi, R. Alizadeh, A. Hivechi, Z. Arabpour, M. Hamidi, C. Delattre, Human olfactory mucosa stem cells delivery using a collagen hydrogel: As a potential candidate for bone tissue engineering, Materials 14 (14) (2021) 3909.

[39] Y.D. Nokoorani, A. Shamloo, M. Bahadoran, H. Moravvej, Fabrication and characterization of scaffolds containing different amounts of allantoin for skin tissue engineering, Sci. Rep. 11 (1) (2021) 1–20.

[40] S. Alizadeh, P. Farshi, N. Farahmandian, Z.A. Ahovan, A. Hashemi, M. Majidi, A. Azadbakht, M. Darestanifarahani, K.S. Sepehr, S.C. Kundu, Synergetic dual antibiotics-loaded chitosan/poly (vinyl alcohol) nanofibers with sustained antibacterial delivery for treatment of XDR bacteria-infected wounds, Int. J. Biol. Macromol. (2022).

[41] Z.A. Ahovan, S. Khosravimelal, B.S. Eftekhari, S. Mehrabi, A. Hashemi, S. Eftekhari, P.B. Milan, M. Mobaraki, A.M. Seifalian, M. Gholipourmalekabadi, Thermo-responsive chitosan hydrogel for healing of full-thickness wounds infected with XDR bacteria isolated from burn patients: In vitro and in vivo animal model, Int. J. Biol. Macromol. 164 (2020) 4475–4486.

[42] A. Azadbakht, S. Alizadeh, Z.A. Ahovan, Z. Khosrowpour, M. Majidi, S. Pakzad, S. Shojaei, N.P.S. Chauhan, M. Jafari, M. Gholipourmalekabadi, Chitosan-placental ECM composite thermos-responsive hydrogel as a biomimetic wound dressing with angiogenic property, Macromol. Biosci. 2200386 (2022).

[43] A. Ghaffarieh, F. Ghaffarpasand, M. Dehghankhalili, N. Honarpisheh, S. Nirumandi, N. Tanideh, Effect of transcutaneous electrical stimulation on rabbit corneal epithelial cell migration, Cornea 31 (5) (2012) 559–563.

[44] S. Hibino, K. Nishida, D. Serrano, H. Hayashi, N. Maeda, Y. Tano, The Effect of Ethanol Treatment on Rabbit Corneal Epithelium: A Histological Study, Invest. Ophthalmol. Vis. Sci. 44 (13) (2003) 3834.

[45] P. Ramhormozi, J. Mohajer Ansari, S. Simorgh, M.J.J.o.B.C. Nobakht, Research, Bone marrow-derived mesenchymal stem cells combined with simvastatin accelerates burn wound healing by activation of the Akt/mTOR pathway, 41(5) (2020) 1069-1078.

[46] A. Mogaldea, K. Theodoridis, T. Goecke, I. Tudorache, A. Haverich, S. Cebotari, A. Hilfiker, Assessment of cytocompatibility and mechanical properties of detergent-decellularized ovine pericardial tissue, Int. J. Artif. Organs 42 (11) (2019) 628–635.

[47] R. Sarvari, P. Keyhanvar, S. Agbolaghi, L. Roshangar, E. Bahremani, N. Keyhanvar, M. Haghdoost, S.H. Keshel, A. Taghikhani, N. Firouzi, A comprehensive review on methods for promotion of mechanical features and biodegradation rate in amniotic membrane scaffolds, J. Mater. Sci. - Mater. Med. 33 (3) (2022) 1–26.

[48] L. Hao-ran, L. Xiao, N. Xin-ye, Y. Hui-lin, Y. Lei, A novel hydrogel-polydimethylsiloxane elastomer for wound dressing application, Ferroelectrics 523 (1) (2018) 104–111.

[49] H. Liu, Z. Zhou, H. Lin, J. Wu, B. Ginn, J.S. Choi, X. Jiang, L. Chung, J.H. Elisseeff, S. Yiu, Synthetic nanofiber-reinforced amniotic membrane via interfacial bonding, ACS Appl. Mater. Interfaces 10 (17) (2018) 14559–14569.

[50] S. Gobinathan, S.S. Zainol, S.F. Azizi, N.M. Iman, R. Muniandy, H.N. Hasmad, M.R. b. Yusof, S. Husain, H. Abd Aziz, Y. Lokanathan, Decellularization and genipin crosslinking of amniotic membrane suitable for tissue engineering applications, J. Biomater. Sci. Polym. Ed. 29 (17) (2018) 2051–2067.

[51] Z. Zhou, D. Long, C.-C. Hsu, H. Liu, L. Chen, B. Slavin, H. Lin, X. Li, J. Tang, S. Yiu, Nanofiber-reinforced decellularized amniotic membrane improves limbal stem cell transplantation in a rabbit model of corneal epithelial defect, Acta Biomater. 97 (2019) 310–320.

[52] J.-Y. Lai, Carbodiimide cross-linking of amniotic membranes in the presence of amino acid bridges, Mater. Sci. Eng. C 51 (2015) 28–36.

[53] E. Spoerl, G. Wollensak, F. Reber, L. Pillunat, Cross-linking of human amniotic membrane by glutaraldehyde, Ophthalmic Res. 36 (2) (2004) 71–77.

[54] M. Gholipourmalekabadi, A. Samadikuchaksaraei, A.M. Seifalian, A.M. Urbanska, H. Ghanbarian, J.G. Hardy, M.D. Omrani, M. Mozafari, R.L. Reis, S.C. Kundu, Silk fibroin/amniotic membrane 3D bi-layered artificial skin, Biomed. Mater. 13 (3) (2018) 035003.

[55] A. Hadipour, V. Bayati, M. Rashno, M. Orazizadeh, Aligned Poly (ε-caprolactone) Nanofibers Superimposed on Decellularized Human Amniotic Membrane Promoted Myogenic Differentiation of Adipose Derived Stem Cells, Cell Journal (yakhteh) 23 (6) (2021) 603.

[56] H.N. Hasmad, R. Bt Hj Idrus, N. Sulaiman, Y. Lokanathan, Electrospun Fiber-Coated Human Amniotic Membrane: A Potential Angioinductive Scaffold for Ischemic Tissue Repair, Int. J. Mol. Sci. 23 (3) (2022) 1743.

[57] T. Hariya, Y. Tanaka, S. Yokokura, T. Nakazawa, Transparent, resilient human amniotic membrane laminates for corneal transplantation, Biomaterials 101 (2016) 76–85.

[58] F. Sales, A. Souza, R. Ariati, V. Noronha, E. Giovanetti, R. Lima, J. Ribeiro, Composite material of PDMS with interchangeable transmittance: Study of optical, mechanical properties and wettability, Journal of Composites Science 5 (4) (2021) 110.

[59] M. Gholipourmalekabadi, M. Sameni, D. Radenkovic, M. Mozafari, M. Mossahebi-Mohammadi, A. Seifalian, Decellularized human amniotic membrane: how viable is it as a delivery system for human adipose tissue-derived stromal cells? Cell Prolif. 49 (1) (2016) 115–121.

[60] S. Sreekantan, M. Hassan, S. Sundera Murthe, A. Seeni, Biocompatibility and cytotoxicity study of polydimethylsiloxane (PDMS) and Palm oil fuel ash (POFA) sustainable super-hydrophobic coating for biomedical applications, Polymers 12 (12) (2020) 3034.

[61] L. Wang, C. Wang, S. Wu, Y. Fan, X. Li, Influence of the mechanical properties of biomaterials on degradability, cell behaviors and signaling pathways: current progress and challenges, Biomater. Sci. 8 (10) (2020) 2714–2733.

[62] H.-S. Yu, J.-J. Kim, H.-W. Kim, M.P. Lewis, I. Wall, Impact of mechanical stretch on the cell behaviors of bone and surrounding tissues, J. Tissue Eng. 7 (2016) 2041731415618342.

[63] M. Gholipourmalekabadi, N.P.S. Chauhan, B. Farhadihosseinabad, A. Samadikuchaksaraei, Human amniotic membrane as a biological source for regenerative medicine, Perinatal tissue-derived stem cells, Springer2016, pp. 81-105.

[64] M. Gholipourmalekabadi, M. Bandehpour, M. Mozafari, A. Hashemi, H. Ghanbarian, M. Sameni, M. Salimi, M. Gholami, A. Samadikuchaksaraei, Decellularized human amniotic membrane: more is needed for an efficient dressing for protection of burns against antibiotic-resistant bacteria isolated from burn patients, Burns 41 (7) (2015) 1488–1497.

[65] T.Ž. Ramuta, L. Tratnjek, A. Janev, K. Seme, M. Starčič Erjavec, M.E. Kreft, The antibacterial activity of human amniotic membrane against multidrug-resistant bacteria associated with urinary tract infections: New insights from normal and cancerous urothelial models, Biomedicines 9 (2) (2021) 218.

[66] F. Asgari, S. Khosravimelal, M. Koruji, Z.A. Ahovan, A. Shirani, A. Hashemi, H. G. Hamidabadi, N.P.S. Chauhan, L. Moroni, R.L. Reis, Long-term preservation effects on biological properties of acellular placental sponge patches, Mater. Sci. Eng. C 121 (2021) 111814.

[67] P. De La Parra-Colin, A. Gonzalez-De La Torre, R. Franco-Cendejas, A. Gonzalez-Veliz, V. Zarza-Garcia, I.P. Vázquez Mellado Martínez, M.d.L. García Hernández, T. J.J.o.B.C. Barrientos-Gutierrez, Research, Ocular surface characteristics and colonization in a burn center: A prospective cohort study, 43(1) (2022) 43-50.

[68] D. Talreja, C. Muraleedharan, G. Gunathilaka, Y. Zhang, K.S. Kaye, S.K. Walia, A.J. C.E.R. Kumar, Virulence properties of multidrug resistant ocular isolates of Acinetobacter baumannii, 39(7) (2014) 695-704.

[69] S.-P. Wilshaw, J. Kearney, J. Fisher, E. Ingham, Biocompatibility and potential of acellular human amniotic membrane to support the attachment and proliferation of allogeneic cells, Tissue Eng. A 14 (4) (2008) 463–472.

[70] S. Defrere, M. Mestagdt, R. Riva, F. Krier, A. Van Langendonckt, P. Drion, C. Jérôme, B. Evrard, J.P. Dehoux, J.M. Foidart, In vivo biocompatibility of three potential intraperitoneal implants, Macromol. Biosci. 11 (10) (2011) 1336–1345.
[71] D. Meller, M. Pauklin, H. Thomasen, H. Westekemper, K.-P. Steuhl, Amniotic membrane transplantation in the human eye, Dtsch. Arztebl. Int. 108 (14) (2011) 243.
[72] X. Zhao, W. Song, Y. Chen, S. Liu, L. Ren, Collagen-based materials combined with microRNA for repairing cornea wounds and inhibiting scar formation, Biomater. Sci. 7 (1) (2019) 51–62.
[73] C.-Y. Tsai, L.-C. Woung, J.-C. Yen, P.-C. Tseng, S.-H. Chiou, Y.-J. Sung, K.-T. Liu, Y.-H. Cheng, Thermosensitive chitosan-based hydrogels for sustained release of ferulic acid on corneal wound healing, Carbohydr. Polym. 135 (2016) 308–315.
[74] H.M. Razi, N. Mosleh, T. Shomali, N. Tavangar, F. Namazi, Deterioration of wound healing and intense suppression of MMP-9 mRNA expression after short-term administration of different topical glucocorticoids or NSAIDs in an avian model of corneal lesions, Iran. J. Veterin. Res. 22 (3) (2021) 188.
[75] S.G. Kaya, S. Inanc-Surer, G. Cakan-Akdogan, G. Oktay, C.A. Utine, S. Kalyoncu, Roles of matrix metalloproteinases in the cornea: A special focus on macular corneal dystrophy, Med. Drug Discov. 11 (2021) 100095.
[76] J.-H. Chang, N.K. Garg, E. Lunde, K.-Y. Han, S. Jain, D.T. Azar, Corneal neovascularization: an anti-VEGF therapy review, Surv. Ophthalmol. 57 (5) (2012) 415–429.